Lab on a Chip

PAPER

View Article Online
View Journal | View Issue

Cite this: *Lab Chip*, 2025, **25**, 2696

Evaluating migration and cytotoxicity of tissue-resident and conventional NK cells in a 3D microphysiological system using live-cell imaging†

Hyeri Choi,[a] June Ho Shin,[b] Hyeonsu Jo,[c]
John B. Sunwoo*[b] and Nool Li Jeon *[acd]

Received 23rd December 2024,
Accepted 7th April 2025

DOI: 10.1039/d4lc01095g

rsc.li/loc

Natural killer (NK) cells are critical components of the immune response against cancer, recognized for their ability to target and eliminate malignant cells. Among NK cell subsets, intraepithelial ILC1 (ieILC1)-like tissue resident NK (trNK) cells exhibit distinct functional properties and enhanced cytotoxicity compared to conventional NK (cNK) cells, positioning them as promising candidates for cancer immunotherapy. However, the specific roles and mechanisms of these cytotoxic trNK cells within the tumor microenvironment (TME) remain to be further explored. In this study, we utilized a three-dimensional (3D) microphysiological system (MPS) to model the tumor–vascular interface and investigate the distinct capabilities of cytotoxic ieILC1-like trNK and cNK cells within the TME. Through the integration of live-cell imaging and cell-tracking analysis, we quantitatively assessed NK cell migration, tumor infiltration, and cytotoxic activity in real time. Our findings revealed that trNK cells demonstrate enhanced motility, sustained tumor interactions, and superior tumor-killing efficiency compared to cNK cells. This study highlights the unique properties of trNK cells, providing a robust foundation for developing next-generation cancer therapies that harness their potent cytotoxic capabilities.

Introduction

Natural killer (NK) cells, a key component of the innate immune system, play a critical role in immune surveillance by responding to infections and eliminating abnormal cells, including those in early-stage cancer.[1] Representing up to 5–15% of circulating lymphocytes in healthy adults, NK cells are functionally categorized based on their expression of CD56. CD56$^{\text{bright}}$ NK cells are primarily involved in immunoregulation through cytokine production, while CD56$^{\text{dim}}$ NK cells exhibit strong cytotoxic capabilities, directly eliminating target cells.[2] NK cells possess a unique ability to detect cells with reduced MHC class I expression, known as "missing self" recognition, which enables them to eliminate tumor cells that evade detection by T cells. This innate ability, combined with their interaction with adaptive immune cells such as dendritic cells and T cells, positions NK cells as central players in immune defense and cancer immunotherapy.[3]

NK cells can be further divided into conventional NK (cNK) cells, which predominantly circulate in peripheral blood, and tissue-resident NK (trNK) cells, which are localized in tissues such as the liver, uterus, and skin. While cNK cells are specialized for systemic immune responses, trNK cells are uniquely adapted for tissue-specific immune responses. They express markers such as CD103 and CD49a, which enhance tissue retention, adhesion, and localized immune functions.[4,5] These adaptations enable trNK cells to overcome physical barriers in the tumor microenvironment (TME) and perform critical roles in immune surveillance and tumor suppression. A specialized subset of trNK cells shares phenotypic and functional similarities with a subset of innate lymphoid cells (ILC), called intraepithelial ILC1 (ieILC1). These cells express high levels of granzymes and perforin and appear to have the capacity of protect against tumor progression.[6,7] The unique characteristics of ieILC1-like trNK cells, along with their high cytolytic potential in the tumor microenvironment, position them as critical players in localized immune defense and promising candidates for advanced cancer immunotherapy.

The functional capabilities of NK cells have been widely studied, but understanding the distinct roles of NK subsets, particularly ieILC1-like trNK cells, in localized tumor immunity remains challenging. This is largely due to the lack

---

[a] Interdisciplinary Program in Bioengineering, Seoul National University, 1 Gwanak-ro, Gwanak-gu, Seoul 08826, Republic of Korea. E-mail: njeon@snu.ac.kr
[b] Department of Otolaryngology – Head & Neck Surgery, Stanford University, 801 Welch Rd., Stanford, CA 94305, USA. E-mail: sunwoo@stanford.edu
[c] Department of Mechanical Engineering, Seoul National University, 1 Gwanak-ro, Gwanak-gu, Seoul 08826, Republic of Korea
[d] Institute of Advanced Machines and Design (SNU-IAMD), Seoul National University, 1 Gwanak-ro, Gwanak-gu, Seoul 08826, Republic of Korea

† Electronic supplementary information (ESI) available. See DOI: **https://doi.org/10.1039/d4lc01095g**

of *in vitro* models that accurately replicate the complex interactions within human tissues. Microphysiological systems (MPS) have emerged as transformative tools to address this limitation by providing highly controlled, three-dimensional (3D) environments that closely mimic physiological conditions.[8] By integrating tissue-specific features, MPS models enable researchers to replicate key aspects of the TME, such as the tumor–vascular interface, stromal components, and ECM dynamics. Previous studies have demonstrated the potential of MPS to advance our understanding of NK cell biology in various contexts.[9–12] For example, a liver-on-chip model revealed that trNK cells are significantly more effective than cNK cells at preventing metastatic tumor seeding in the liver.[13] Similarly, MPS platforms have been used to investigate memory-like NK cells in head and neck squamous cell carcinoma (HNSCC) by incorporating patient-derived tumor spheroids and immune components into these systems.[14] In our previous work, we developed a vascular network model composed of endothelial cells, tumor cells, and ECM to replicate intricate interactions within the TME.[15] While this model successfully captured NK cell cytotoxic activity across various cancer subtypes, its complexity posed challenges in isolating and quantifying specific NK cell migratory behaviors, emphasizing the need for more streamlined yet physiologically relevant models for precise real-time NK cell analysis.

In this study, we simplified the vascular network model to focus specifically on the tumor–vascular interface, providing an optimized platform for precise quantification of NK cell migration, infiltration, and cytotoxic activity. Using a 3D MPS integrated with live-cell imaging, we replicated the dynamic and spatially confined conditions of the TME to directly compare the functional capabilities of ieILC1-like trNK (herein, called "trNK" cells) and cNK cells. Real-time imaging captured critical processes such as NK cell migration from the vascular wall, tumor infiltration, sustained interactions with tumor cells, and target cell killing. This approach quantitatively validated the superior motility, tissue retention, and tumor-killing efficacy of trNK cells, particularly the ieILC1-like subset, which demonstrated localized immune responses specifically tailored to the TME. In contrast to cNK cells, which rely on systemic circulation and generalized cytokine signaling, trNK cells successfully navigated TME barriers, including the dense extracellular matrix, to deliver highly specific and sustained cytotoxic responses. By integrating MPS with advanced imaging and cell-tracking analysis, this study not only advances our understanding of NK cell biology but also establishes a robust platform for developing next-generation cancer immunotherapies that leverage the unique properties of trNK cells.

Methods and materials

Device fabrication

Compression-molded polystyrene (PS) sheets were injection-molded at R&D Factory (Korea) using a machined and polished aluminum alloy mold core. The process involved a 15-second cycle time, 55 bar injection pressure, 220 °C nozzle temperature, and 130-ton clamping force. The molded microfluidic devices were then bonded to a pressure-sensitive adhesive-coated polycarbonate film (Izsolution, Korea; Cat# PC200). Detailed fabrication and design methods have been provided previously.[16,17]

Cell preparation

Human umbilical vein endothelial cells (HUVECs, Lonza, Switzerland; Cat# C2519a) were cultured in endothelial growth medium-2 (EGM-2, Lonza, Switzerland; Cat# CC-3162). The HNSCC cell line, FaDu cells (ATCC, USA; Cat# HTB-43) were grown in Dulbecco's modified Eagle's medium (DMEM, Gibco, USA; Cat# 11965092) with 10% heat-inactivated fetal bovine serum (Thermo Fisher Scientific, USA; Cat# 16140071) and 1% penicillin/streptomycin (Gibco, USA; Cat# 15140148). All cell types were incubated at 37 °C with 5% CO_2 for three days before application. Cells were detached from culture dishes using 0.25% trypsin–EDTA (HyClone, USA; Cat# SH30042.01). Green fluorescent protein (GFP)-tagged FaDu cells were seeded at 10 000 cells per well in a 96-well round-bottom, ultra-low attachment microplate (Corning, USA; Cat# 7007) to spheroids ranging from 300 to 500 μm for tumor infiltration assays.

NK cell isolation

Human blood samples were obtained from healthy donors through the Stanford Blood Center under a protocol approved by the Stanford Institutional Review Board. All procedures were conducted in accordance with local legislation and institutional guidelines. Written informed consent was obtained from all participants. NK cell enrichment was performed using the RosetteSep NK Cell Enrichment Mixture (Stem Cell Technologies, Canada; Cat# 15065), following a previously published method.[6] To confirm NK cell enrichment, we used flow cytometry to exclude non-NK cells by staining CD3, CD14, CD19, and CD20 (BioLegend, USA; Cat# 300426, 325620, 302218 and 302314, respectively). The enriched NK cells were then cultured at a concentration of 10–20 × 10^6 cells per mL in AIM-V medium (Gibco, USA; Cat# 12055091), supplemented with 25 mL of CTS Immune Cell Serum Replacement (Gibco, USA; Cat# A2596101) and 10 ng mL^{-1} interleukin-15 (IL-15, BioLegend, USA; Cat# 570306) to support NK cell survival and expansion. The culture medium was refreshed every 2 days, with NK cells passaged every 4 days to maintain optimal cell growth and viability.

NK cell differentiation (ieILC1-like trNK)

NK cells were co-cultured with irradiated-PCI-13 cells at an effector-to-target (E : T) ratio of 1 : 2 in AIM-V medium supplemented with CTS and IL-15. To promote differentiation, the culture medium was refreshed every 2 days, and NK cells were passaged every 4 days with irradiated-PCI-13 cells. Surface markers (CD103, CD49a) were monitored on days 3 and 7 using flow cytometry (BD FACSAria™ II SORP) to confirm differentiation into ieILC1-like trNK cell characteristics. Cells were stained with Fixable Viability Dye eFluor 780 (APC-Cy7, eBioscience, USA; Cat# 65-0865-18) for 20 min at 4 °C in the dark, washed with FACS buffer, and stained with a specific antibody mixture for NK cell surface markers: CD45 (BV605, BioLegend, USA; Cat# 368524), CD56 (PE-Cy5, BD Biosciences, USA; Cat# 555517), CD103 (BioLegend, USA; Cat# 350203), and CD49a (BioLegend, USA; Cat# 328314) for 30 min at 4 °C in the dark. After staining, cells were washed again and resuspended in FACS buffer for single-cell sorting. Compensation was performed using single-stained controls for each fluorophore with compensation beads, followed by automated compensation setup in FACSDiva™ Software. CD103 + CD49a + trNK cells were isolated through multiple gating strategies for further *in vitro* experiments using the MPS (Fig. S1†).

Hydrogel patterning and cell seeding

To prepare for cell seeding, all devices underwent plasma treatment at 70 W for 3 min (Harrick Plasma, USA) to increase surface hydrophilicity. A 50 μL gel mixture, composed of HNSCC cell suspension (2×10^6 cells per mL) and 2.5 mg mL^{-1} bovine fibrinogen solution, was mixed with 1 μL of 0.25 U mL^{-1} bovine thrombin solution and immediately injected (1 μL per central channel) before full polymerization. After polymerization, HUVEC cell suspension (2×10^6 cells per mL) was injected into a side channel. The devices were tilted 90° and incubated at 37 °C for 20 min and to allow the HUVEC cells to settle directly above the gel-patterned central channel. EGM-2 medium was then added to the media reservoirs, and confluent monolayers formed after 2 days, at which point trNK and cNK cells were introduced. For the spheroid model, each spheroid was embedded in a fibrin gel mixture with NK cells and injected through the central hole to position it centrally within the device. Migration and infiltration assays for trNK and cNK cells toward cancer cells were conducted after 2 days of co-culture.

Real-time NK cell-mediated cytotoxic assay

2D NK cell killing assays were performed using the Avatar AI system (AVATAR™, Xcell Biosciences, USA), which evaluates cell killing based on impendence measurements. FaDu cells were seeded onto a 96-well plate embedded with electrodes and subsequently loaded into the AI system to initiate the screening experiment. NK cell efficiency was assessed over at E : T ratios of 1 : 5, 1 : 2, 1 : 1, 2 : 1 and 5 : 1. Real-time impedance measurements were continuously recorded throughout the assay to monitor cell activity. The collected data were processed using XcellSoft software to determine the percentage of specific lysis for each NK cell subset.

For 3D NK cell killing assays, experiments were conducted using a MPS at an E : T ratio of 1 : 1. Killing activity was monitored for 48 hours using the Celloger Mini Plus imaging system (Curiosis, Korea), with images captured at 5-minute intervals. FaDu cells and NK cells were stained with Alexa Fluor 488 Anti-EpCAM antibody (BioLegend, USA; Cat# 324210) and CellTrace™ Far Red Cell Proliferation kit (Thermo Fisher Scientific, USA; Cat# C34572), respectively. Propidium iodide (PI, Thermo Fisher Scientific, USA; Cat# P3566) was used to identify dead cells. The same devices were cultured in the Avatar system under controlled TME conditions (1% oxygen, 2 PSI pressure, and 37 °C), and endpoint images were captured.

Real-time migration assays

NK cell migration toward tumor cells was assessed using a tumor–vascular interface model within a 3D MPS environment. Real-time live-cell imaging was conducted with Zeiss Cell Observer SD Spinning Disk Confocal microscope to capture and analyze NK cell migration paths. Quantification analysis of NK cell interactions with endothelial and tumor cells, including migration speed, distance traveled, and infiltration capacity of both cNK and trNK cells,[18,19] was performed using Python modules, primarily OpenCV. Additionally, Numpy and Matplot libraries were employed for computations and visualizations. All code is available publicly, with assembled scripts available upon request. As a preliminary study to assess NK cell behavior in hypoxic conditions, the same devices were cultured in the Avatar system under controlled TME conditions (1% oxygen, 2 PSI pressure, and 37 °C), and endpoint images were captured.

Cell tracking methods

Immune cell trajectories were analyzed using a Python-based algorithm with OpenCV libraries, based on time-lapse microscopy imaging. The tracking process involved cell segmentation, feature extraction, trajectory linking, and motion analysis to quantify the movement of cNK and trNK cells in the tumor microenvironment. Raw time-lapse images were preprocessed using Gaussian filtering to reduce noise and enhance cell boundaries. Individual immune cells were then segmented using a threshold-based approach combined with morphological operations to separate overlapping cells. After segmentation, cell centroids were detected and assigned unique identifiers.

To construct cell trajectories, frame-to-frame matching was performed using a nearest-neighbor approach based on Euclidean distance. The algorithm linked detected cell positions across consecutive frames, ensuring that each trajectory represented a single cell's movement over time. Any cells that temporarily disappeared and later reappeared were re-associated if their new position was within a predefined distance threshold. Following trajectory linking, motion parameters including velocity, displacement, and migration persistence were computed. The total migration distance of each cell was calculated by summing the frame-to-frame displacements, while the migration persistence index was determined as the ratio of net displacement to total distance traveled.

Statistical analysis

Experiments were repeated at least three times under consistent conditions, with results presented as mean ± SE. ImageJ was used for image processing, and statistical analysis was conducted using Student's *t*-tests. Data visualization and graphing were performed using Origin 2021. Statistically significant differences ($p < 0.05$) are indicated.

Results and discussion

Microphysiological system design for charactering NK cell behavior

To compare the functional characteristics of two NK cell subsets—cNK and trNK cells—NK cells were isolated from peripheral blood samples obtained from healthy human donors. These cells were cultured *in vitro* with IL-15, a cytokine that supports NK cell survival, activation, and proliferation.[20] Differentiation of cNK cells into ieILC1-like trNK cells was achieved using a well-established, previously published protocol, which involved co-culturing cNK cells with irradiated PCI-13 cells while maintaining a continuous supply of IL-15 to simulate the tissue-specific environmental cues (Fig. 1A).[6] The transition to the trNK phenotype was confirmed by the increased expression of tissue-residency markers CD49a and CD103, with a significant proportion of double-positive cells observed between day 3 and day 7 of co-culture. Flow cytometric data (Fig. S1†) revealed a consistent and progressive upregulation of these markers, validating the differentiation protocol. Highly purified populations of both cNK and ieILC1-like trNK cells were confirmed prior to each experimental assay to ensure phenotypic stability and reproducibility, which are critical for consistent downstream functional analyses. Distinct marker profiles between cNK and trNK populations, as illustrated by representative flow cytometry plots, further underscored the phenotypic different between the subsets (Fig. 1B).

We developed a tumor–vascular interface model using a MPS to investigate the dynamic behaviors of individual NK cell subsets within the TME. This simplified model was designed to replicate key components of the TME, emphasizing the interactions between an endothelial cell monolayer and cancer cells in a controlled 3D

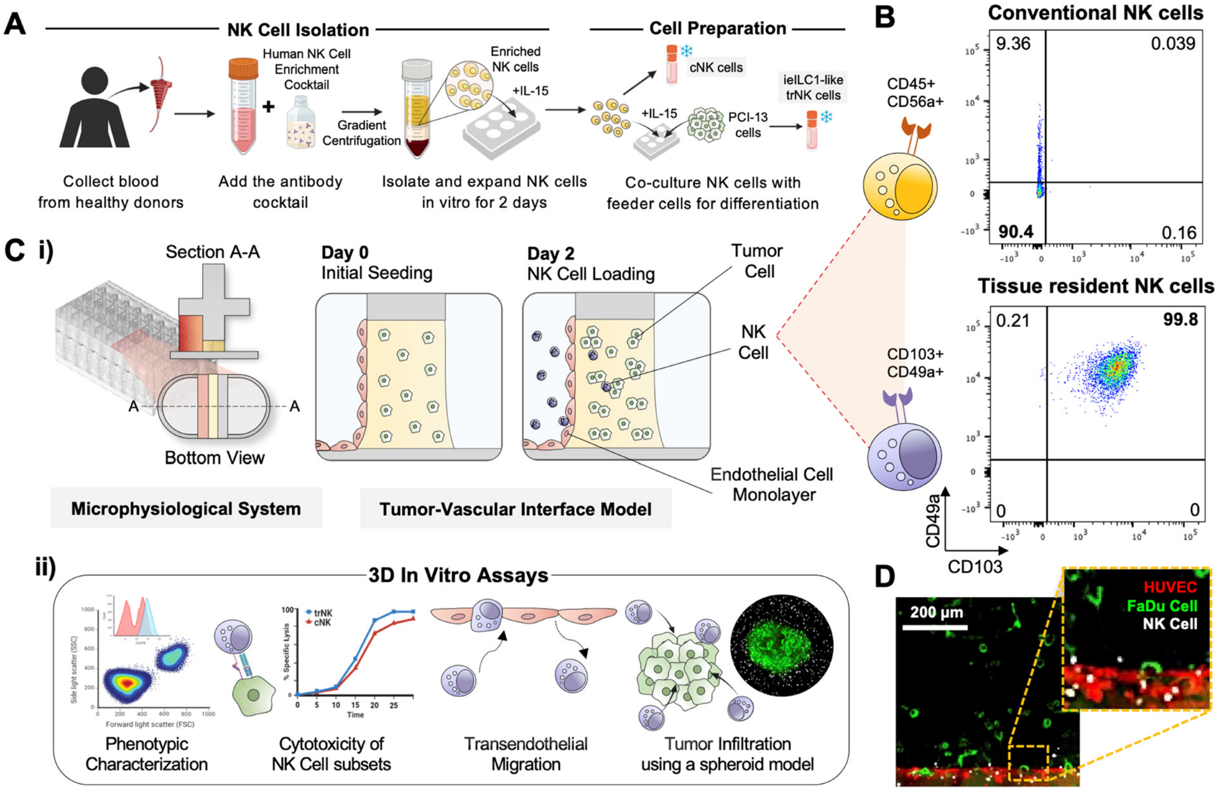

Fig. 1 Design of a microphysiological system-based tumor model for NK cell characterization. A. Protocol for isolating NK cells from human blood and differentiating them into ieILC-1-like trNK cells. After isolation, NK cells were expanded *in vitro* for 2 days and then either cryopreserved as cNK cells or co-cultured with PCI-13 cells for 8 days to promote differentiation into ieILC1-like trNK cells. B. Analysis of major surface markers (CD103, CD49a) distinguishing cNK and trNK cells. C. (i) Schematic of the tumor–vascular interface model in a three-channel MPS. Tumor cells were encapsulated in hydrogels in the central channel, with endothelial cells attached to the side of the gel to form a monolayer on day 0. NK cells were introduced into the channel on day 2 to establish the tumor–vascular interface model. (ii) Functional characterization through cytotoxicity assays, and migration/infiltration analysis. D. Confocal image showing the endothelial monolayer (red), cancer cells (green), and NK cells (white).

environment. For the experimental setup, each well of the MPS contained three interconnected microchannels, with two channels utilized for the tumor–vascular interface model: one containing dispersed HNSCC cells encapsulated in a hydrogel matrix to mimic tumor tissue, and the other simulating a vascular compartment with an endothelial monolayer. Purified cNK or trNK cells were introduced into the endothelial channel to monitor their migration across the endothelial barrier and into the hydrogel matric containing HNSCC cells (Fig. 1C(i)). The model could also be refined by integrating tumor spheroids or pre-co-cultured cancer and NK cells, allowing for an expanded scope and more comprehensiveness of functional evaluations. Such refinements enable simultaneous analyses of NK cell subset-specific behaviors, including migration, infiltration, and cytotoxic effects on cancer cells within a 3D environment (Fig. 1C(ii)). To ensure optimal experimental conditions, the model was cultivated for 2 days before introducing NK cells to allow sufficient time for the formation of a stable endothelial cell monolayer and stabilization of tumor cells within the hydrogel matrix. Following this stabilization period, cNK and trNK cells were introduced separately into the endothelial channel, as illustrated in Fig. 1D. Throughout the study, this tumor–vascular interface model demonstrated its utility in elucidating the functional differences between cNK and trNK cells, providing valuable insights into their district roles within the TME.

Enhanced cytotoxicity of trNK cells in a 3D microenvironment

The enhanced cytotoxic potential of NK cells has been demonstrated in previous studies using mouse models and 2D *in vitro* systems.[21–23] To further investigate their behavior in a 3D environment using the MPS, NK cells and cancer cells were co-cultured within hydrogels at an E : T ratio of 1 : 1 (Fig. 2A(i)). This co-culture was monitored over 2 days using a live-cell imaging system, which enabled real-time detection of red fluorescence while maintaining optimal culture conditions in an incubator. This setup allowed for dynamic observation of cytotoxic activity and the distinct morphological features of NK cell subsets. During the co-culture, cNK cells predominantly maintained a rounded morphology, whereas trNK cells exhibited an elongated shape and progressively adhered to the ECM, suggesting their adaptability for tissue infiltration (Fig. 2A(ii)). These morphological differences were accompanied by distinct functional differences: trNK cells engaged in significantly closer and more sustained interactions with cancer cells, while cNK cells exhibited limited attachment and engagement. The enhanced adhesion and prolonged contact

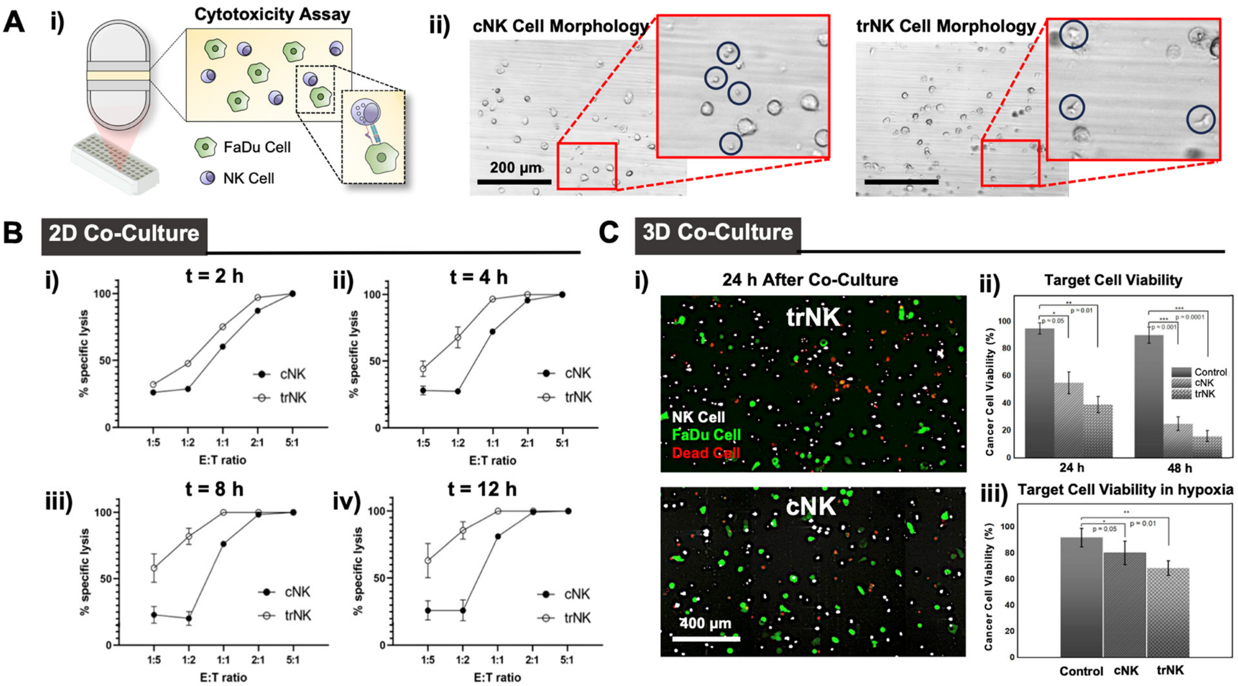

Fig. 2 Enhanced cytotoxic activity of trNK cells compared to cNK cells. A. (i) Configuration of the microchannel setup, containing ECM, FaDu cells, and NK cells. (ii) Brightfield images showing circular-shaped cNK cells and elongated trNK cells. B. Specific lysis of target cancer cells by different NK cell subsets—conventional NK (cNK) and tissue-resident NK (trNK) cells—at various E : T ratios: (i) 2 hours, (ii) 4 hours, (iii) 8 hours, and (iv) 16 hours after co-culture. The graphs demonstrate that trNK cells consistently exhibit higher cytotoxic activity compared to cNK cells across all time points (n = 4 wells per each ratio). C. 3D cytotoxicity assay using the MPS. (i) Fluorescence images 24 hours after co-culture showing cancer cell death (red) and viable NK cells (green). (ii) Bar graph quantifies tumor cell viability at 24 and 48 hours, indicating a significant reduction in viability with trNK cells compared to cNK cells. (iii) Cancer cell viability under hypoxic conditions at 24 hours, showing sustained higher cytotoxic activity of trNK cells compared to cNK cells (n = 15 wells per condition).

of trNK cells with cancer cells suggests the potential for higher cytotoxic efficacy in tissue-like environments.[24] These dynamic interactions were captured in Videos S1 and S2,† highlighting the ability of trNK cells to infiltrate and interact effectively within the 3D microenvironment.

The cytotoxic activity of these NK cells was initially validated in a 2D environment using impedance-based cell activity measurements. Although the enhanced cytotoxicity of trNK cells has been well-documented in previous studies,[6] we repeated this validation to ensure the functionality of our isolated NK cells in this experimental setup. Time-course data revealed the percentage of specific cancer cell lysis by cNK and trNK cells at various time points (2, 4, 8, and 12 hours) and E:T ratios (1:5, 1:2, 1:1, 2:1, and 5:1). Consistent with prior findings, trNK cells exhibited significantly higher killing activity compared to cNK cells across all time points, with the difference being most pronounced at 8 and 12 hours, reflecting their sustained cytotoxic efficacy (Fig. 2B(iii and iv)). This re-validation confirms the reliability and functionality of our trNK cell isolation and further reinforces their performance in cancer cell killing.

In the 3D environment, fluorescence images showed a greater number of dead cancer cells (red fluorescence) in co-cultures with trNK cells compared to those with cNK cells (Fig. 2C(i)). Quantitative analysis indicated a significant reduction in tumor cell viability in the trNK group, with viability decreasing to approximately 38% at 24 hours and 15% at 48 hours. In contrast, viability in the cNK group remained at approximately 53% and 25% at these respective time points (Fig. 2C(ii)). These results suggest that while the ECM in 3D environments may delay cytotoxic activity,[12] it does not diminish the superior efficacy of trNK cells. Under TME conditions mimicking hypoxia (1% oxygen) using a hypoxic incubator (Avatar AI),[25] trNK cells continued to exhibit higher killing capacity compared to cNK cells (Fig. 2C(iii)). This preliminary study provides a foundation for further investigation into NK cell cytotoxicity under hypoxic conditions in both 2D and 3D environments. The findings strongly suggest that trNK cells possess significantly enhanced cancer-killing capabilities relative to cNK cells, demonstrating superior efficacy over time and across various E:T ratios.

Comparison of tumor infiltration in a tumor spheroid model

Using a modified MPS specifically designed to capture tumor spheroids in the center of the microchannel,[17] we assessed tumor infiltration by different NK cell subsets. Tumor spheroids composed of GFP-tagged FaDu (HNSCC) cells were cultured at the center of the microchannel, with NK cells surrounding the spheroid in the ECM (Fig. 3A(i)). Regions of interest (ROIs) were defined to encompass the entire tumor spheroid, and multilayered confocal imaging was employed

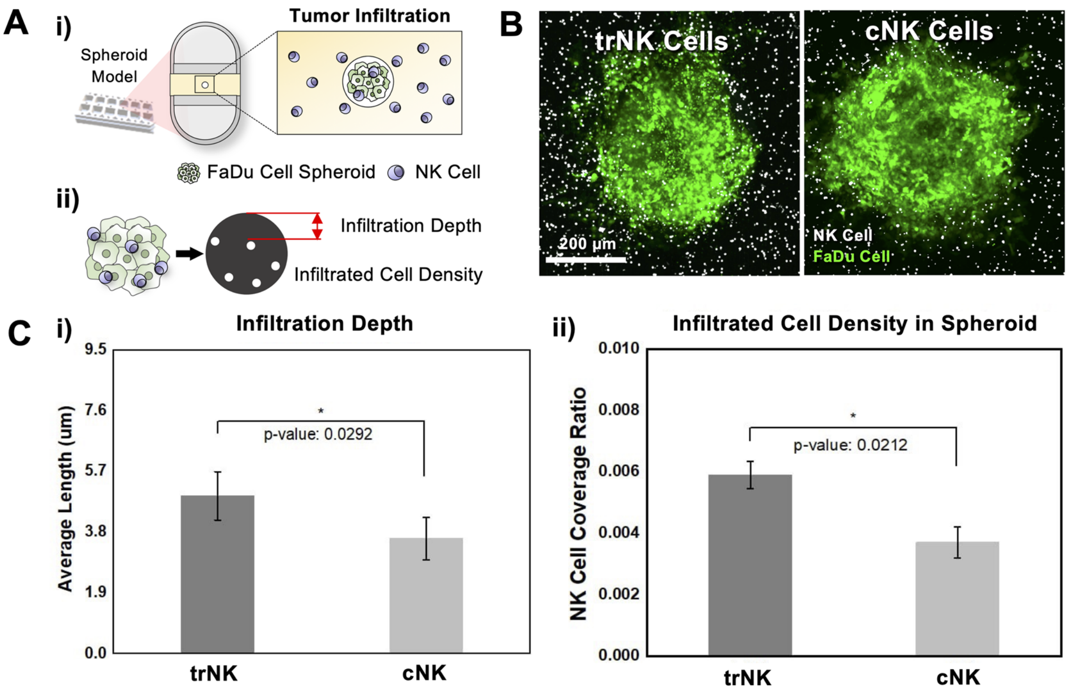

Fig. 3 Comparison of trNK and cNK cell infiltration in tumor spheroid models. A. (i) Schematic representation of the tumor infiltration model. The model captures a tumor spheroid positioned in a central well, with NK cells surrounding it. (ii) Key parameters for evaluating NK cell infiltration ability include infiltration depth and the density of infiltrated cells, allowing comparison between trNK and cNK cell subsets. B. Confocal images showing individual NK cells (white) interacting with the tumor spheroids (green). Data were normalized to account for differences in spheroid size. C. Graphs illustrating (i) the increased density of infiltrated cells within the spheroids and (ii) the greater infiltration depth achieved by trNK cells (n = 9 total spheroids per condition).

to confirm that NK cells not only adhered to the surface but also penetrated into the tumor spheroid. This approach enabled precise evaluation of two key parameters: the infiltration depth, measured as the distance from the spheroid surface to the location of the NK cell, and the infiltrated cell density, calculated as the proportion of NK cells within the tumor spheroid region relative to the total spheroid area (Fig. 3A(ii)).

Comparative analysis based on Fig. 3B revealed that trNK cells exhibited both greater infiltration depth and higher infiltrated cell density within the tumor spheroid compared to cNK cells (Fig. 3C(i and ii)). These results suggest that trNK cells are more effectively attracted to tumor cells, demonstrate superior migratory ability within the ECM, and can penetrate the tumor spheroid more efficiently. Statistical analysis confirmed the significance of these findings, with p-values of 0.0112 and 0.0352 for infiltration depth and infiltrated cell density, respectively.

While the enhanced cytotoxic potential of trNK cells has been extensively studied, their infiltration behavior, particularly that of ieILC1-like trNK cells within tumors, has not been thoroughly investigated. This model offers valuable insights into the mechanisms driving trNK cell infiltration and their interactions with cancer cells. The interaction of trNK cells with the ECM and cancer cells likely enhances their engagement and cytotoxic activity, potentially driven by the expression of adhesion molecules such as CD103 and CD49a.[21] The observed increased in trNK cell infiltration may result from the interaction between the CD103 surface marker on trNK cells and E-cadherin, an epithelial cell receptor expressed on cancer cells.[26,27] This interaction likely supports adhesion and penetration into the TME, though its precise mechanisms require further investigation.

Enhanced migratory capacity of ieILC1-like trNK cells across different conditions

The tumor–vascular interface model was utilized to investigate the extravasation and migration behaviors of cNK and trNK cells toward cancer cells under various conditions. NK cell migration involves a series of sequential steps, including chemoattraction, rolling, and transendothelial migration (Fig. 4A(i)). As outlined earlier, the experimental setup for this model included the migration of NK cells through a monolayer of HUVECs toward HNSCC cancer cells, and following the introduction of NK cells, their migration behavior was continuously monitored in real-time using live-cell confocal microscopy for 2 days, with endpoint images

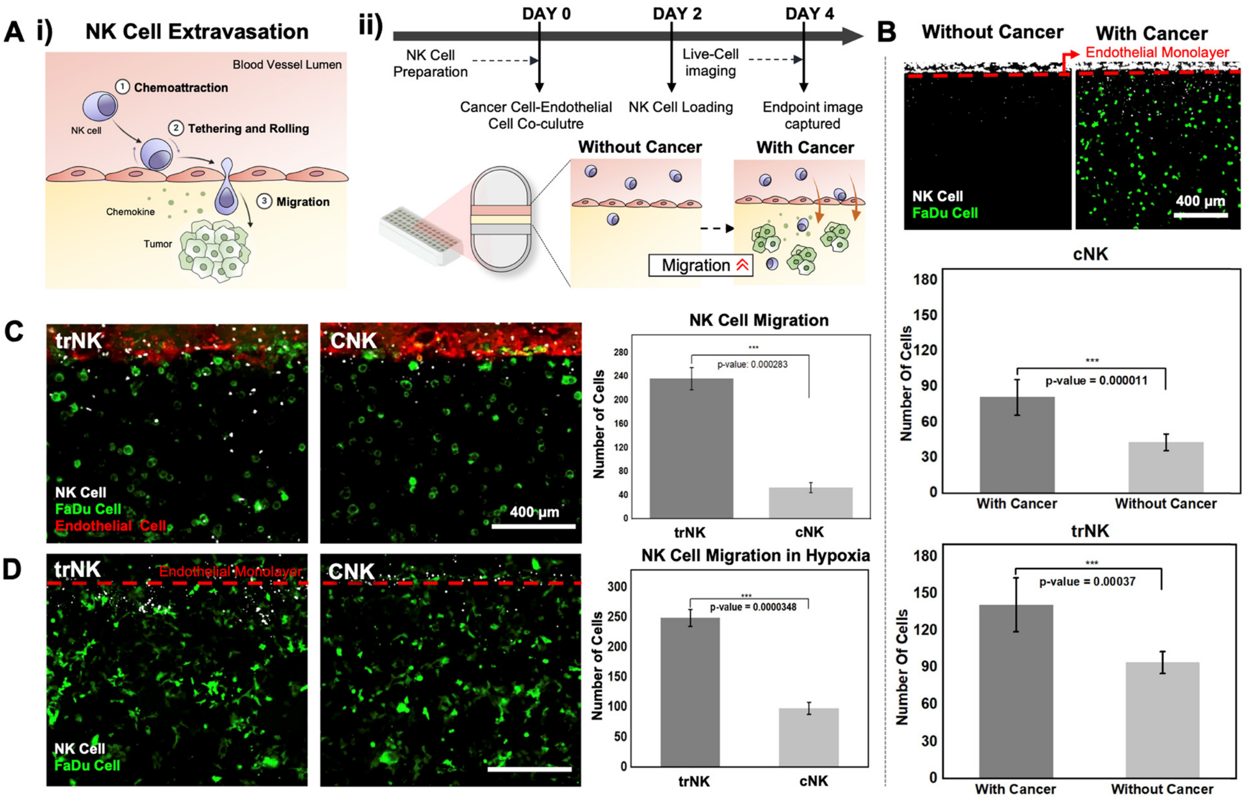

Fig. 4 NK cell extravasation and migration assay using a tumor–vascular interface model. A. (i) Schematic illustrating NK cell extravasation, from initial chemoattraction to migration toward tumor cells. (ii) Schematic representation of the experimental setup for studying NK cell migration and extravasation using an organ-on-chip model, illustrating the migration of NK cells through endothelial layers toward cancer cells B. Quantification of NK cells (white) in the ECM region in the absence and presence of cancer cells (green), showing a significant increase in number of NK cells when tumor cells are present. C. Comparison of cNK and trNK cell (white) migration through the endothelial cell layer (red) toward cancer cells (green). D. Migration of cNK and trNK cells (white) toward cancer cells (green) under hypoxic conditions (n = 30 wells per condition).

captured on the final day of the experiment (day 4). The initial co-culture conditions included configurations with and without cancer cells in the central channel to assess the impact of cancer cell presence on NK cell attraction (Fig. 4A(ii)). Quantitative analysis revealed that trNK cells were significantly more effective at traversing the endothelial barrier, showing a pronounced increase in migration toward cancer cells compared to conditions without cancer cells (*p*-value = 0.000037). Similarly, cNK cells also demonstrated enhanced migration in the presence of cancer cells (*p*-value = 0.000011). Endpoint imaging confirmed that both NK cell subsets showed increased migration when cancer cells were present, aligning with expectations (Fig. 4B).

When cancer cells were present in the migration assay, trNK cells demonstrated significantly greater migratory ability through the ECM toward tumor sites compared to cNK cells, emphasizing their enhanced responsiveness to cancer cells (Fig. 4C). Fluorescence imaging revealed a substantially higher concentration of trNK cells (white) at the endothelial barrier (red) and within the cancer cell region (green). In contrast, cNK cells traversed the endothelial barrier at an average of 40 cells per field of view, whereas trNK cells reached approximately 240 cells per field of view. The significantly higher number of trNK cells extravasating into the TME compared to cNK cells was highly statistically significant (*p*-value = 0.000283). These results indicate that trNK cells are considerably more efficient at navigating to tumor sites, whereas cNK cells showed a relatively limited migration capacity.

Under hypoxic conditions, trNK cells once again outperformed cNK cells in migration capacity, as evidenced by both the confocal images and bar graph data (*p*-value = 0.0000348) (Fig. 4D). Despite the additional challenges posed by hypoxia, trNK cells maintained their enhanced migratory behavior, showing a marked increase in the number of cells penetrating the endothelial monolayer and interacting with cancer cells. Some previous studies have suggested that hypoxia enhances immune cell migration.[28,29] This model could serve as a useful tool for investigating the mechanisms and molecular pathways underlying their behavior in 3D hypoxic environments, which are not yet fully understood.

The results clearly demonstrate the distinct migratory behaviors of trNK and cNK cells toward cancer cells in the TME. The superior migration and extravasation capacity of trNK cells can be attributed to their tissue-resident phenotype, which likely enables them to effectively sense chemokine gradients, traverse the endothelial barrier, and infiltrate tumor tissues. The enhanced adaptability of trNK cells likely arises from their high expression of chemokine receptors. Notably, trNK cells express significantly higher levels of CXCR6, CXCR4, and CCR5 compared to cNK cells.[30–32] These chemokine interactions may facilitate the efficient migration of trNK cells toward tumor sites. Further studies and analyses on chemokines produced by cancer cells in this model, as well as their corresponding chemokine receptors on NK cells, should be conducted for a more comprehensive discussion, which will be addressed in future research. The enhanced functionality of trNK cells highlights their remarkable adaptability and efficacy in the TME, even under challenging conditions such as hypoxia.

Real-time trajectory analysis of ieILC1-like trNK cell migration

The sequence of events highlighting extravasation, target recognition, and tumor cell killing by NK cells was captured through real-time migration monitoring (Fig. 5A(i)). Within 12 hours, trNK cells were observed crossing the endothelial monolayer, recognizing cancer cells, and initiating tumor cell killing. The migration speed of NK cells in tissue varies depending on factors such as tissue type, microenvironment, and external stimuli, including chemokine gradients or the presence of target cells.[31] In our experiments, both NK cell types achieved migration speeds that were well within the expected range for hydrogel environments,[33] and trNK cells demonstrated a slightly higher average migration speed compared to cNK. Speed profiles showed that trNK cells migrated slightly faster than cNK cells, achieving speeds of approximately 12 μm min^{-1} compared to 10.5 μm min^{-1} for cNK cells (Fig. 5A(ii) and S2†). Moreover, the total distances traveled by the two subsets differ markedly. The trNK cells covered approximately 18 000 μm during live-cell imaging, while cNK cells traveled significantly shorter distances (Fig. 5A(iii)). Videos S3 and S4† provide dynamic visualizations of trNK and cNK cell migration within the TME, respectively.

Detailed tracking of individual NK cells revealed distinct movement patterns within the TME (Fig. 5B). The trajectories of five highly active trNK cells demonstrated extensive, exploratory movement, with individual trNK cells covering distances up to 5802.67 μm. The color-coded trajectories highlighted their high mobility and frequent directional changes of trNK cells, suggesting active engagement with cancer cells and exploratory tracking behavior. In contrast, the most active cNK cells exhibited shorter, more constrained movement patterns with the longest trajectory reaching 146 μm. The inset graphs in the trNK and cNK trajectory figures represent localized movement patterns of selected immune cells, with their *Y*-position anchored at 0 for comparison. trNK cells show variations in the *y*-axis, while cNK cells remain more confined with minimal vertical displacement. These patterns align with the main trajectory graphs. The immune cell clustering analysis reveals distinct spatial behaviors between cNK and trNK cells. cNK cells exhibit a more confined distribution, forming fewer but denser clusters, while trNK cells display a more dispersed clustering pattern, suggesting greater mobility and interaction within the tumor environment. The presence of multiple distinct trNK clusters indicates higher engagement with the target tumor cells, whereas cNK cells remain more aggregated (Fig. S3 and S4†). Further analysis showed that trNK cells showed

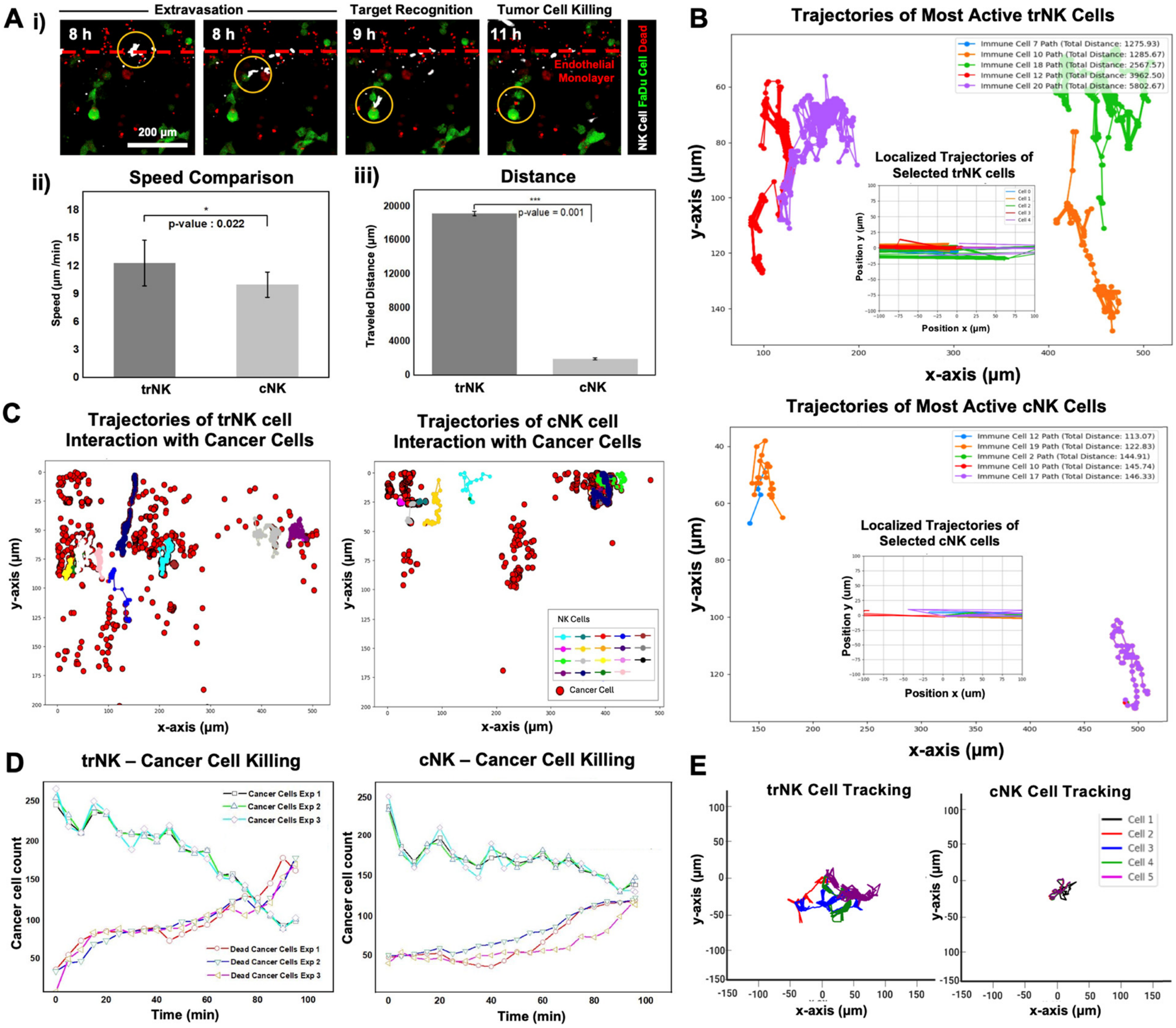

Fig. 5 Migration analysis using real-time live-cell imaging. A. (i) Live-cell imaging of trNK cell behaviors, including extravasation, tumor cell recognition, and tumor cell killing. (ii) Bar graphs comparing migration speeds of the two NK cell subsets (n = 20). (iii) Total distance traveled by each subset (n = 5). B. Trajectories of most active trNK cells (top) and cNK cells (bottom), with color-coded lines representing distinct immune cell paths to visualize their migration dynamics. The inset graphs display localized trajectories of the cells with the Y-position normalized to emphasize relative displacement. C. Plots illustrating the dynamic movement patterns of immune cells toward cancer cells (red dots), highlighting their ability to navigate and engage with target cells. D. Cancer cell counts over time, showing live and dead cancer cell numbers across three experiments in the presence of either trNK or cNK cells. t = 0 denotes the point at which NK cells initiate cancer cell killing following their transendothelial migration. E. Trajectories of five individual trNK and cNK cells, tracked over time along x and y coordinates, demonstrating their movement patterns and interactions with cancer cells.

widespread and directional trajectories toward tumor cell clusters (Fig. 5C). In comparison, cNK cells showed limited spatial coverage and interaction with dispersed cancer cells, suggesting a static, localized engagement strategy. Our tracking algorithm identifies cancer cells and measures their Euclidean distance from nearby NK cells. If this distance falls below a predefined threshold, the cancer cell is classified as interacting with an NK cell and appears in the graphs. The higher cancer cell density in the trNK condition suggests increased interactions with trNK cells compared to cNK cells. These findings indicate that trNK cells are significantly more adept at exploring the TME and engaging with cancer cells, demonstrating superior spatial coverage and tumor-seeking behavior. Conversely, the restricted mobility of cNK cells reduces their effectiveness in targeting dispersed cancer cells.

Cancer cell killing by trNK cells occurred at a significantly higher rate compared to cNK cells across all experiments (Fig. 5D). The cumulative cancer cell death count increased more rapidly in experiments involving trNK cells, reflecting their higher killing efficiency over time. The cancer cell death rates induced by cNK and trNK cells (Fig. S5A and B†) further underscore the significantly greater mobility and cytotoxicity of trNK cells relative to cNK cells. The trendlines and intensity plots (Fig. S5C–E†) distinguish live, dead, and NK cells based on their intensity levels, providing a quantitative measure of cancer cell death in live-cell imaging. The killing dynamics showed that trNK cells consistently eliminated more cancer cells during each even, as indicated by a progressive and steeper increase in the number of dead cancer cells over time. While both NK cell subsets contributed to significant cancer cell death, trNK cells demonstrated markedly greater efficacy in navigating the TME and executing cytotoxic functions. These findings highlight that trNK cells are not only more mobile but also significantly more effective in real-time targeting and elimination of cancer cells.

The movement tracking data provided further insights into the distinct behaviors of trNK cells and cNK cells (Fig. 5E). The contrasting trajectories and movement ranges revealed fundamental behavioral differences between these subsets, which also likely contribute to their divergent cytotoxic capabilities. The broader movement range of trNK cells enabled more frequent interactions with cancer cells, thereby enhancing their killing efficiency. Their variable trajectories, covering wider ranges along both the x and y axes, demonstrated a more exploratory movement pattern that facilitated the efficient search for and engagement with cancer cells within the TME. In contrast, cNK cells exhibited restricted movement with narrower ranges along both axes, limiting their ability to interact with and eliminate cancer cells. The constrained mobility of cNK cells likely reduces their ability to explore the microenvironment and effectively target cancer cells.

These live-cell imaging results suggest that the enhanced motility and engagement ability of trNK cells play a critical role in their cytotoxic efficiency. The observed longer migration distances, faster speeds, and dynamic exploratory behavior of trNK cells demonstrate their capacity to efficiently navigate and migrate toward cancer cells. These attributes are essential for effective immune surveillance and cancer cell targeting. In contrast, the restricted movement and limited exploratory behavior of cNK cells emphasize their dependence on systemic immune responses rather than localized tissue targeting. The confined trajectories of cNK cells suggest a reduced adaptability to the dynamic and dense TME. This study offered a comprehensive quantification of trNK cell migration and extravasation through endothelial barriers, emphasizing their exceptional ability to target and interact with cancer cells within the TME, using the MPS for the first time.

Future perspectives and therapeutic applications

Using our tumor–vascular interface model and real-time live-cell imaging, we quantitatively demonstrated that the trNK cells navigate tissue barriers and engage tumor cells more effectively than cNK cells. These findings align with prior research that emphasize the role of NK cells in suppressing tumor progression and metastatic seeding.[34] Such results underscore the therapeutic potential of trNK cells, particularly for targeting solid tumors where localized and sustained immune responses are critical.

Despite these promising findings, several limitations must be addressed. First, while our *in vitro* MPS model provides a robust platform for simulating the TME, it does not fully replicate the complexity of *in vivo* tumor–immune interactions, including vascular dynamics, immune suppression, and stromal heterogeneity. Second, this study primarily focused on the functional differences between ieILC1-like trNK and cNK cells, without evaluating the influence of other immune populations that could modulate NK cell behavior. Third, while live-cell imaging provided key insights, the molecular mechanisms underlying trNK cell specialization and tissue residency require further investigation and validation *in vivo*. Future research should focus on overcoming these limitations by integrating advanced multi-omics techniques to validate and expand the findings. Single-cell RNA sequencing and in-depth proteomic analyses could provide a more granular understanding of the molecular pathways driving trNK cell behavior. Exploring combinatorial approaches, such as engineering cNK cells to express trNK-specific markers, could also pave the way for enhanced NK cell-based therapies.

Additionally, this study emphasizes the need to investigate genes unique to ieILC1-like trNK cells, such as ITGAE (CD103), ITGA1 (CD49a), CXCR6, and NCR2, which play pivotal roles in tissue retention, migration, and cytotoxicity. Shared cytotoxic genes, including GZMA, GZMB, GZMH, PRF1, and GNLY, reflect conserved killing mechanisms across NK subsets, while trNK-specific integrin-related genes reinforce their tissue-adaptive functions.[30,35,36] Elevated expression of CD103 and CD49a enables efficient tumor infiltration, even in the presence of dense ECM barriers. Investigating the interaction between CD103 and E-cadherin as a critical adhesion mechanism, particularly through live-cell imaging with CD103 blockade treatments, could yield further insights. Furthermore, the chemokine receptor CXCR6 plays a crucial role in trNK migration and retention, underscoring their functional specialization. Integrating multiplex cytokine secretion assays with our MPS model could validate the chemoattractant signals influencing NK cell migration.

Overall, this study highlights the unique therapeutic potential of trNK cells in cancer immunotherapy. Their superior mobility, infiltration, and cytotoxicity make them promising candidates for targeting solid tumors. By leveraging their distinct properties and addressing current limitations, future therapeutic strategies could overcome the challenges of dense TMEs and enhance the efficacy of NK cell-based therapies.

Conclusions

We utilized a 3D MPS to model the TME, focusing on the tumor–vascular interface, to investigate the distinct functional capabilities of ieILC1-like trNK cells compared to conventional cNK cells. Our findings demonstrated that trNK cells exhibit superior motility, traveling at higher speeds and infiltrating tumors more efficiently than cNK cells in a 3D environment, as quantitatively validated through live-cell imaging. This enhanced ability to localize and sustain interactions with cancer cells significantly amplifies the cytotoxic efficacy of trNK cells within the TME. This study underscores the therapeutic potential of ieILC1-like trNK cells as a highly promising candidate for targeted cancer immunotherapy while establishing a foundational 3D tumor model as a valuable platform for advancing cancer immunotherapy strategies.

Data availability

The data supporting this article have been included as part of the ESI.†

Author contributions

HC: conceptualization, data curation, formal analysis, funding acquisition, investigation, methodology, software, resources, validation, visualization, writing – original draft. JHS: investigation, methodology. HJ: resources, writing – review & editing. JS: conceptualization, funding acquisition, project administration, supervision, writing – review & editing. NLJ: conceptualization, funding acquisition, project administration, supervision, writing – review & editing.

Conflicts of interest

There are no conflicts to declare.

Acknowledgements

This research was supported by a grant of the Korea Health Technology R&D Project through the Korea Health Industry Development Institute (KHIDI), funded by the Ministry of Health & Welfare, Republic of Korea (grant number: HI19C1352), and by a grant from the National Research Foundation of Korea (NRF), funded by the Ministry of Science and ICT (MSIT), Republic of Korea (grant number: 2021R1A3B1077481 and RS-2024-00441103 (the Bio & Medical Technology Development Program)). The work was also supported by a grant from the National Institutes of Health, USA (R35DE030054) to J. B. S. We would also like to acknowledge support from the Flow Cytometry Core Facility at the Stanford Institute for Stem Cell Biology and Regenerative Medicine (Lokey Stem Cell Research Building) for NK cell sorting and flow cytometric analysis.

References

1 M. A. Caligiuri, Human natural killer cells, *Blood*, 2008, **112**(3), 461–469.

2 A. G. Freud, B. L. Mundy-Bosse, J. Yu and M. A. Caligiuri, The Broad Spectrum of Human Natural Killer Cell Diversity, *Immunity*, 2017, **47**(5), 820–833.

3 K. Rezvani, R. Rouce, E. Liu and E. Shpall, Engineering natural killer cells for cancer immunotherapy, *Mol. Ther.*, 2017, **25**(8), 1769–1781.

4 H. Peng and Z. Tian, Diversity of tissue-resident NK cells, in *Seminars in immunology*, Elsevier, 2017, vol. 31, pp. 3–10.

5 D. K. Sojka, B. Plougastel-Douglas, L. Yang, M. A. Pak-Wittel, M. N. Artyomov, Y. Ivanova, C. Zhong, J. M. Chase, P. B. Rothman and J. Yu, Tissue-resident natural killer (NK) cells are cell lineages distinct from thymic and conventional splenic NK cells, *elife*, 2014, **3**, e01659.

6 U. Y. Moreno-Nieves, J. K. Tay, S. Saumyaa, N. B. Horowitz, J. H. Shin, I. A. Mohammad, B. Luca, D. C. Mundy, G. S. Gulati and N. Bedi, Landscape of innate lymphoid cells in human head and neck cancer reveals divergent NK cell states in the tumor microenvironment, *Proc. Natl. Acad. Sci. U. S. A.*, 2021, **118**(28), e2101169118.

7 S. Maddineni, J. L. Silberstein and J. B. Sunwoo, Emerging NK cell therapies for cancer and the promise of next generation engineering of iPSC-derived NK cells, *J. Immunother. Cancer*, 2022, **10**(5), e004693.

8 V. Carannante, M. Wiklund and B. Önfelt, In vitro models to study natural killer cell dynamics in the tumor microenvironment, *Front. Immunol.*, 2023, **14**, 1135148.

9 M. Marzagalli, G. Pelizzoni, A. Fedi, C. Vitale, F. Fontana, S. Bruno, A. Poggi, A. Dondero, M. Aiello and R. Castriconi, A multi-organ-on-chip to recapitulate the infiltration and the cytotoxic activity of circulating NK cells in 3D matrix-based tumor model, *Front. Bioeng. Biotechnol.*, 2022, **10**, 945149.

10 O. T. Nguyen, P. M. Misun, C. Lohasz, J. Lee, W. Wang, T. Schroeder and A. Hierlemann, An immunocompetent microphysiological system to simultaneously investigate effects of anti-tumor natural killer cells on tumor and cardiac microtissues, *Front. Immunol.*, 2021, **12**, 781337.

11 M. Campisi, S. E. Shelton, M. Chen, R. D. Kamm, D. A. Barbie and E. H. Knelson, Engineered microphysiological systems for testing effectiveness of cell-based cancer immunotherapies, *Cancers*, 2022, **14**(15), 3561.

12 D. Park, K. Son, Y. Hwang, J. Ko, Y. Lee, J. Doh and N. L. Jeon, High-throughput microfluidic 3D cytotoxicity assay for cancer immunotherapy (CACI-IMPACT platform), *Front. Immunol.*, 2019, **10**, 1133.

13 R. Fahrner, M. Gröger, U. Settmacher and A. S. Mosig, Functional integration of natural killer cells in a microfluidically perfused liver on-a-chip model, *BMC Res. Notes*, 2023, **16**(1), 285.

14 J. M. Ayuso, M. Farooqui, M. Virumbrales-Muñoz, K. Denecke, S. Rehman, R. Schmitz, J. F. Guerrero, C. Sanchez-de-Diego, S. A. Campo and E. M. Maly, Microphysiological model reveals the promise of memory-like natural killer cell immunotherapy for HIV±cancer, *Nat. Commun.*, 2023, **14**(1), 6681.

15 J. Song, H. Choi, S. K. Koh, D. Park, J. Yu, H. Kang, Y. Kim, D. Cho and N. L. Jeon, High-throughput 3D in vitro tumor vasculature model for real-time monitoring of immune cell infiltration and cytotoxicity, *Front. Immunol.*, 2021, **12**, 733317.

16 J. Yu, S. Lee, J. Song, S.-R. Lee, S. Kim, H. Choi, H. Kang, Y. Hwang, Y.-K. Hong and N. L. Jeon, Perfusable micro-vascularized 3D tissue array for high-throughput vascular phenotypic screening, *Nano Convergence*, 2022, **9**(1), 16.

17 J. Ko, J. Ahn, S. Kim, Y. Lee, J. Lee, D. Park and N. L. Jeon, Tumor spheroid-on-a-chip: a standardized microfluidic culture platform for investigating tumor angiogenesis, *Lab Chip*, 2019, **19**(17), 2822–2833.

18 H. Shoval, A. Karsch-Bluman, Y. Brill-Karniely, T. Stern, G. Zamir, A. Hubert and O. Benny, Tumor cells and their crosstalk with endothelial cells in 3D spheroids, *Sci. Rep.*, 2017, **7**(1), 10428.

19 A. L. Martinez, M. J. Shannon, S. E. Eisman, E. Hegewisch-Solloa, A. N. Asif, T. A. Ebrahim and E. M. Mace, Quantifying human natural killer cell migration by imaging and image analysis, in *Natural Killer (NK) Cells: Methods and Protocols*, Springer, 2022, pp. 129–151.

20 M. A. Cooper, J. E. Bush, T. A. Fehniger, J. B. VanDeusen, R. E. Waite, Y. Liu, H. L. Aguila and M. A. Caligiuri, In vivo evidence for a dependence on interleukin 15 for survival of natural killer cells, *Blood*, 2002, **100**(10), 3633–3638.

21 D. K. Sojka, Z. Tian and W. M. Yokoyama, Tissue-resident natural killer cells and their potential diversity, in *Seminars in immunology*, Elsevier, 2014, vol. 26, pp. 127–131.

22 T. Le, R. K. Reeves and L. R. McKinnon, The functional diversity of tissue-resident natural killer cells against infection, *Immunology*, 2022, **167**(1), 28–39.

23 H. X. Aw Yeang, S. J. Piersma, Y. Lin, L. Yang, O. N. Malkova, C. Miner, A. S. Krupnick, W. C. Chapman and W. M. Yokoyama, Cutting edge: human CD49e− NK cells are tissue resident in the liver, *J Immunol.*, 2017, **198**(4), 1417–1422.

24 H. Sun, C. Sun, W. Xiao and R. Sun, Tissue-resident lymphocytes: from adaptive to innate immunity, *Cell. Mol. Immunol.*, 2019, **16**(3), 205–215.

25 A. Emami Nejad, S. Najafgholian, A. Rostami, A. Sistani, S. Shojaeifar, M. Esparvarinha, R. Nedaeinia, S. Haghjooy Javanmard, M. Taherian and M. Ahmadlou, The role of hypoxia in the tumor microenvironment and development of cancer stem cell: a novel approach to developing treatment, *Cancer Cell Int.*, 2021, **21**, 1–26.

26 G. H. Ran, Y. Q. Lin, L. Tian, T. Zhang, D. M. Yan, J. H. Yu and Y. C. Deng, Natural killer cell homing and trafficking in tissues and tumors: from biology to application, *Signal Transduction Targeted Ther.*, 2022, **7**(1), 205.

27 B. D. Shields, B. Koss, E. M. Taylor, A. J. Storey, K. L. West, S. D. Byrum, S. G. Mackintosh, R. Edmondson, F. Mahmoud and S. C. Shalin, Loss of E-cadherin inhibits CD103 antitumor activity and reduces checkpoint blockade responsiveness in melanoma, *Cancer Res.*, 2019, **79**(6), 1113–1123.

28 M. Parodi, F. Raggi, D. Cangelosi, C. Manzini, M. Balsamo, F. Blengio, A. Eva, L. Varesio, G. Pietra and L. Moretta, Hypoxia modifies the transcriptome of human NK cells, modulates their immunoregulatory profile, and influences NK cell subset migration, *Front. Immunol.*, 2018, **9**, 2358.

29 I. Garcés-Lázaro, R. Kotzur, A. Cerwenka and O. Mandelboim, NK cells under hypoxia: the two faces of vascularization in tumor and pregnancy, *Front. Immunol.*, 2022, **13**, 924775.

30 E. Hashemi and S. Malarkannan, Tissue-resident NK cells: development, maturation, and clinical relevance, *Cancers*, 2020, **12**(6), 1553.

31 G. Bernardini, F. Antonangeli, V. Bonanni and A. Santoni, Dysregulation of chemokine/chemokine receptor axes and NK cell tissue localization during diseases, *Front. Immunol.*, 2016, **7**, 402.

32 J. E. Melsen, G. Lugthart, A. C. Lankester and M. W. Schilham, Human circulating and tissue-resident CD56bright natural killer cell populations, *Front. Immunol.*, 2016, **7**, 262.

33 P. E. Olofsson, L. Brandt, K. E. Magnusson, T. Frisk, J. Jaldén and B. Önfelt, A collagen-based microwell migration assay to study NK-target cell interactions, *Sci. Rep.*, 2019, **9**(1), 10672.

34 S.-Y. Wu, T. Fu, Y.-Z. Jiang and Z.-M. Shao, Natural killer cells in cancer biology and therapy, *Mol. Cancer*, 2020, **19**, 1–26.

35 S. Roma, L. Carpen, A. Raveane and F. Bertolini, The dual role of innate lymphoid and natural killer cells in cancer. From phenotype to single-cell transcriptomics, functions and clinical uses, *Cancers*, 2021, **13**(20), 5042.

36 Y. Yu, The function of NK cells in tumor metastasis and NK cell-based immunotherapy, *Cancers*, 2023, **15**(8), 2323.